Supplemental information

Cell-cell adhesion impacts epithelia response to substrate stiffness: Morphology and gene expression

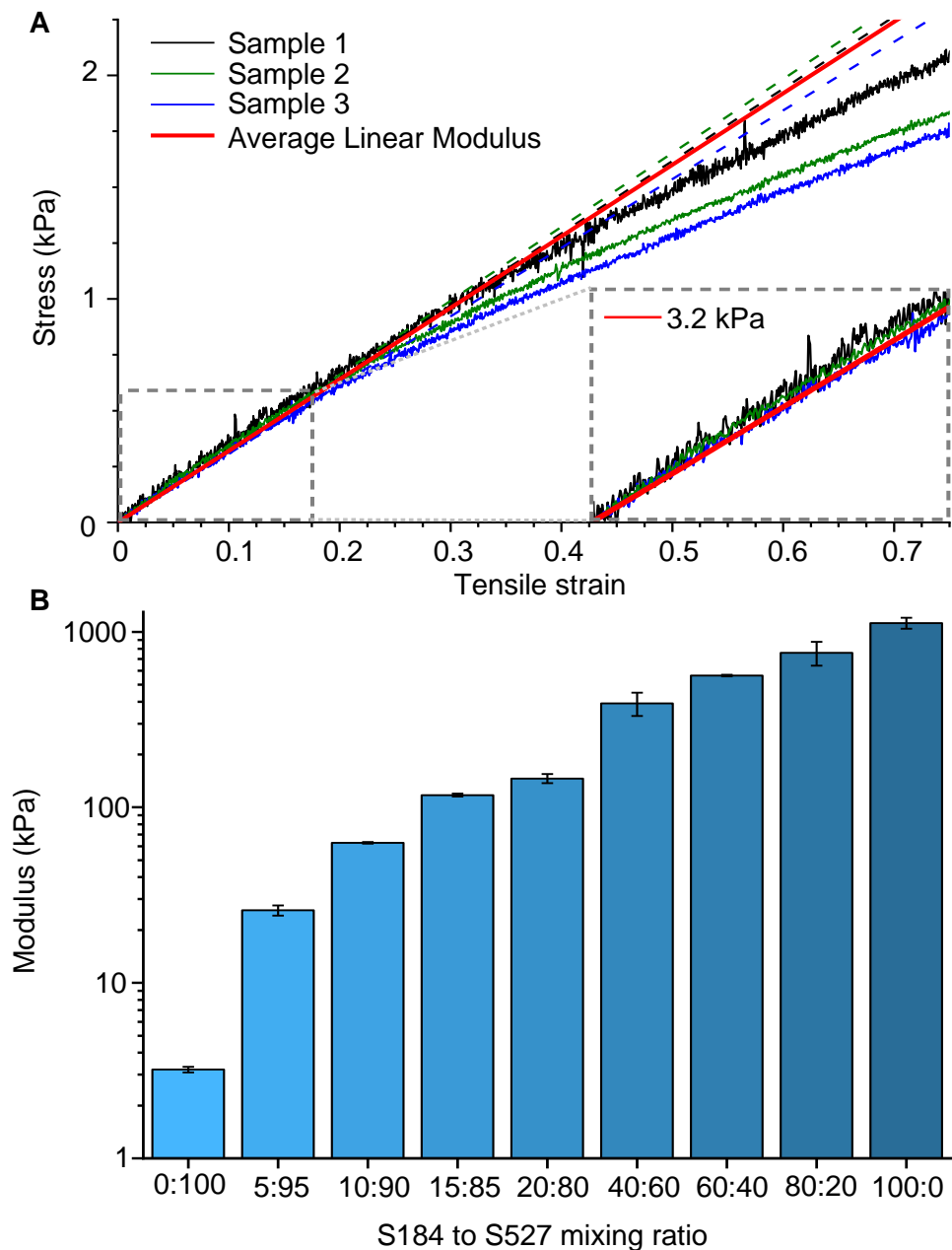David Choi, Zachary Gonzalez, Sum Yat Ho, Alexandra Bermudez, and Neil Y.C. Lin

Figure S1: (A) A stress-strain curve for manufactured S527 (3.2 kPa) samples shows that samples have a mean elastic modulus of 3.2 kPa within the linear region (dashed line box). Our stress-strain curves also indicate a modulus consistency between independent samples and a relatively wide linear regime (up to ~ 30%), which suggests that this formulation can accurately recreate the same stiffness despite variation in yield behaviours. (B) By repeating the mechanical measurement for all tested substrate samples, we created a bar chart for summarizing the overall range of explored moduli. While it is possible to create substrates within a vast range of stiffnesses, the drastic increase with each additional 5% increment of S184 shows that it is difficult to finely tune the modulus with this fabrication method.
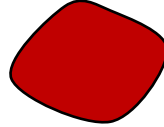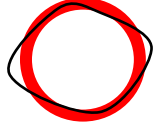
Measurement	Definition	Schematic
Area	Measured space occupied by a single cell in a confluent layer	
Perimeter	The total length of the cell boundary of a single cell in a confluent layer	
Aspect Ratio	Division of the longest measured axis of a cell by the perpendicular short axis	
Circularity	A calculated measure of how round a cell is. Calculated using $4\pi Area/Perimeter^2$	

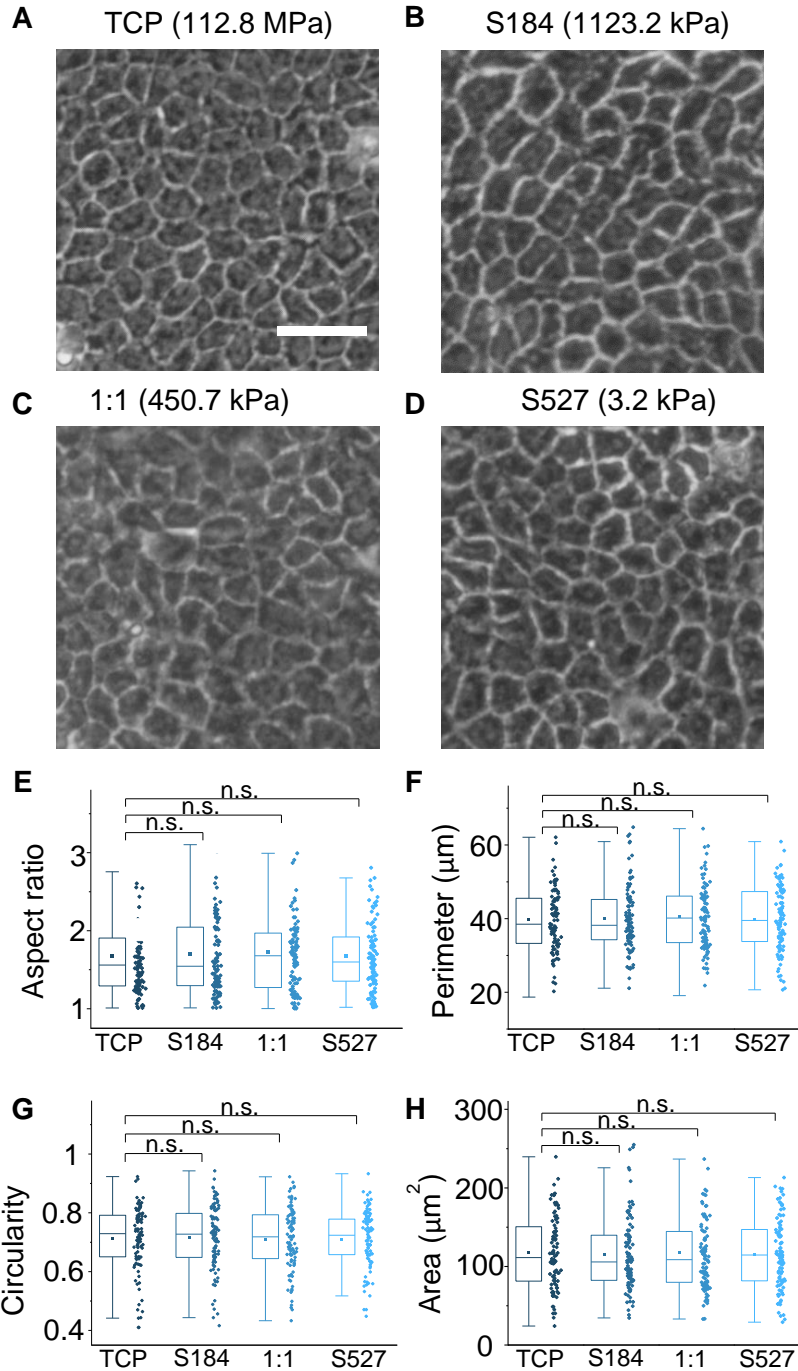**Figure S2**. Definitions for each morphology quantification metric used.

Figure S3: (A-D) Phase contrast images of cells grown on TCP, S184, 1:1 blend of S184 and S527, and S527 reveal no significant morphological differences across substrate stiffness for confluent samples. Scale bar = 110 μm. Aspect ratio (E), perimeter (F), circularity (G), and cell area (G) were calculated by outlining and measuring individual cells from the obtained images for each of the four substrates. This quantification shows that full confluency masks differences in morphology due to substrate stiffness. ; For (E)-(H), n=100.
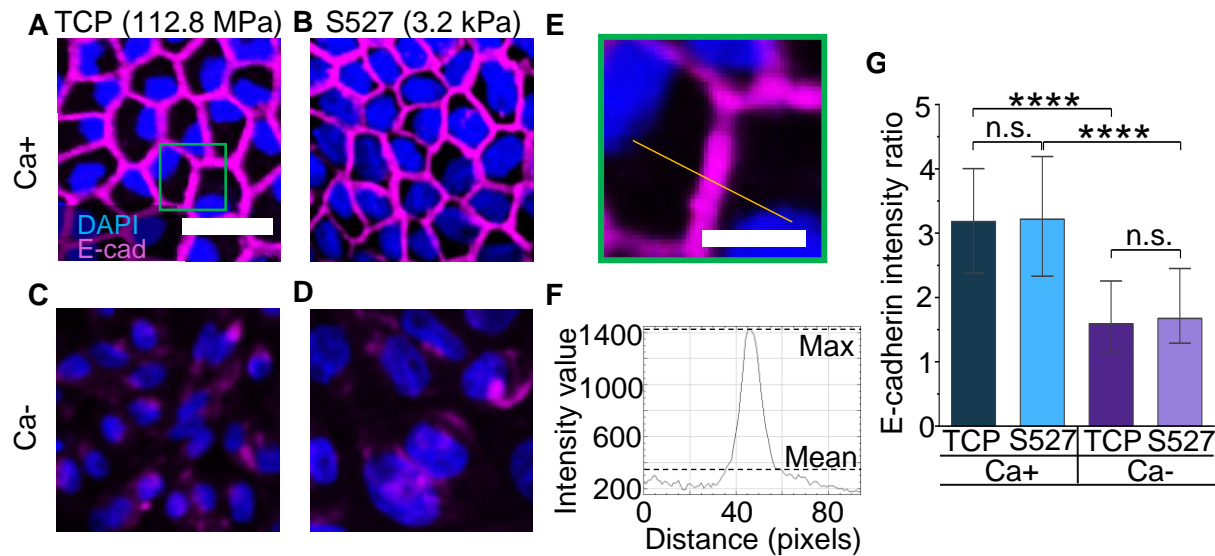
Figure S4: (**A-B**) E-cadherin was found to be localized to cell junctions in confluent monolayers on both TCP and S527 substrates. (**C-D**) Lack of E-cadherin junctional enrichment under the Ca- condition in cells on both substrates supports Ca- treatment as an effective method for perturbing cell-cell adhesions. (**E**) E-cadherin quantifications were performed using line scan analysis with fixed line length of 93 pixels (14.88 µm) drawn across the intercellular junction. Following previous studies, measuring intensity across the line quantifies the max (junctional) and mean (cytoplasmic) intensities. The junctional localization is approximated as the max-to-mean ratio. This method has been shown to be insensitive to the image background intensity and imaging condition variations (1-4). The field of view (green box) was chosen from Fig. S4A. (**F**) An example intensity profile shows the mean (352.36) and maximum (1396.24) intensities of the E-cadherin signal in Fig. S4E. (**G**) Junctional E-cadherin intensity ratio for each condition was quantified by normalizing the maximum intensity by the mean background for each cell junction. No significant differences were observed between substrate stiffnesses under either calcium condition. This indifference in cadherin junctional localization for confluent monolayers suggest that intercellular adhesion strength is not strongly influenced by the substrate stiffness, supporting our finding that the establishment of intercellular junctions masks the substrate stiffness effect. (A) Scale bar = 30 µm. (E) Scale bar = 10 µm. For (G), n=25. * $p \leq 0.05$, ** $p \leq 0.01$, *** $p \leq 0.001$, **** $p \leq 0.0001$.
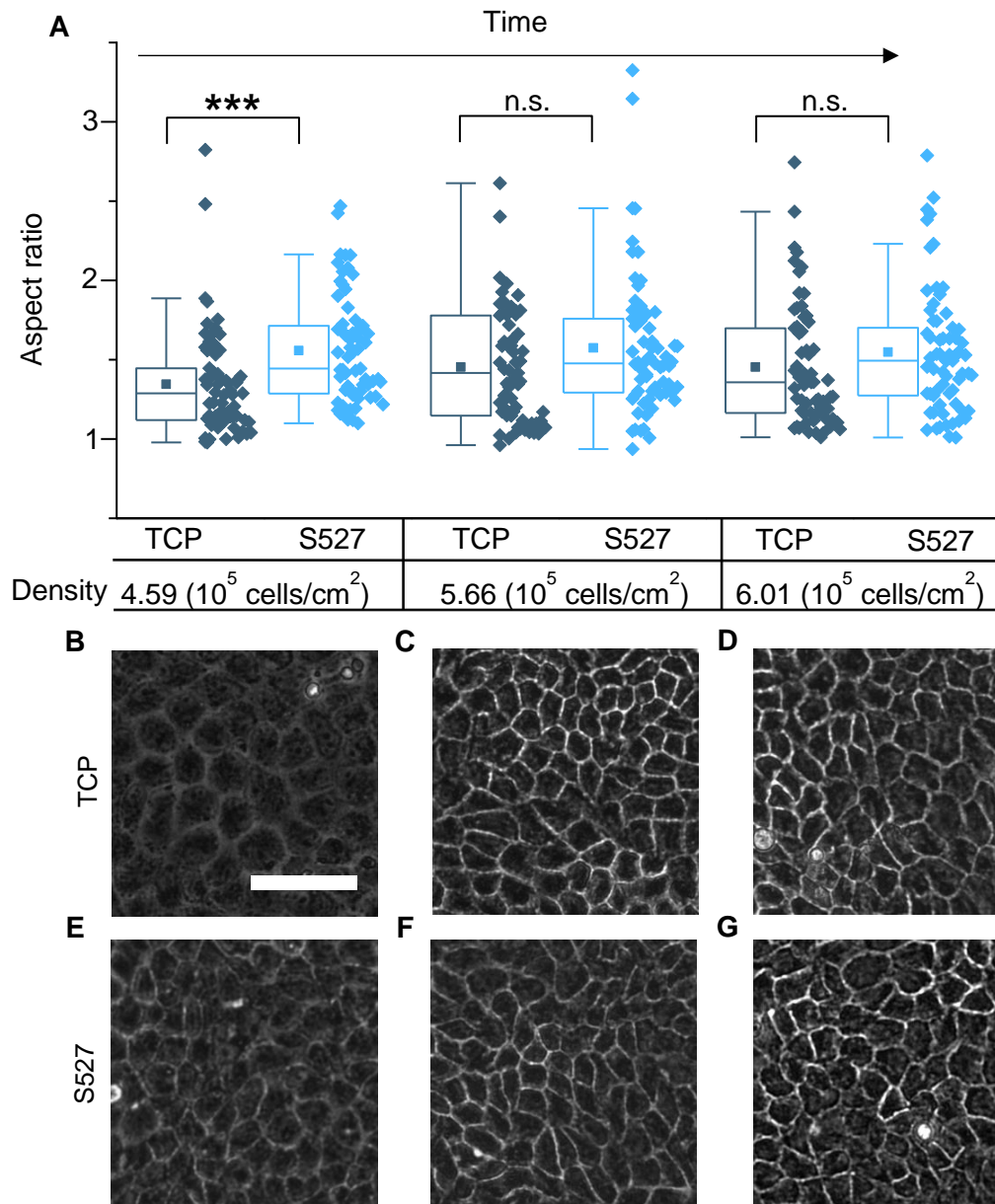
Figure S5: Time lapse images were taken of cells grown on TCP and S527 upon cultures reaching 100% confluence. (A) Aspect ratio measurements reveal that as cells proliferate and increase in cell-cell adhesion, the difference in aspect ratio becomes insignificant. This result is likely due to stronger cell-cell adhesions forming over time as epithelial cells transition from a confluent to a contact inhibited state. Representative images are also shown for cells grown on TCP (B-D) and S527 (E-G). As cells become more packed, their cell-cell contacts establish, as shown by the brightening of cell boundaries.; For (A), n=65. Scale bar = 50 micron. * p≤0.05, ** p≤0.01, *** p≤0.001.

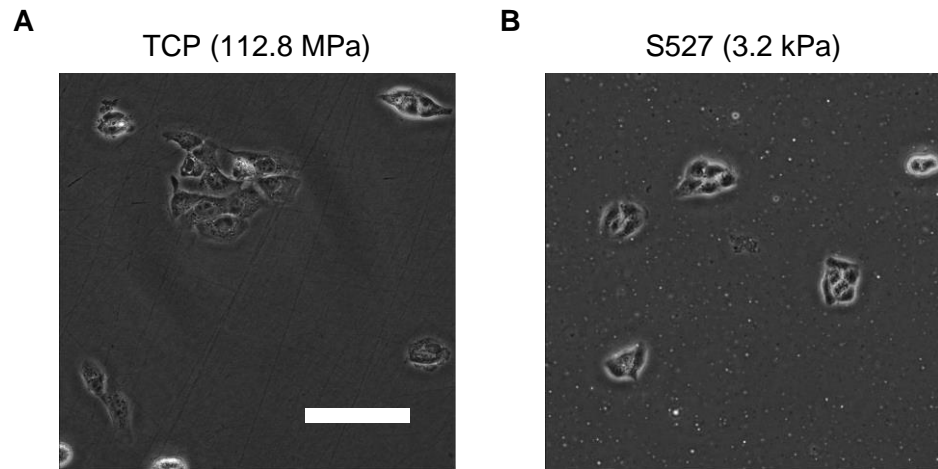**A**
TCP (112.8 MPa)

B
S527 (3.2 kPa)

Figure S6: (A-B) Phase contrast images of cells before lysing to obtain mRNA data for Fig. 1D show the low cell density of the non-confluent state. Scale bar = 50 μm.
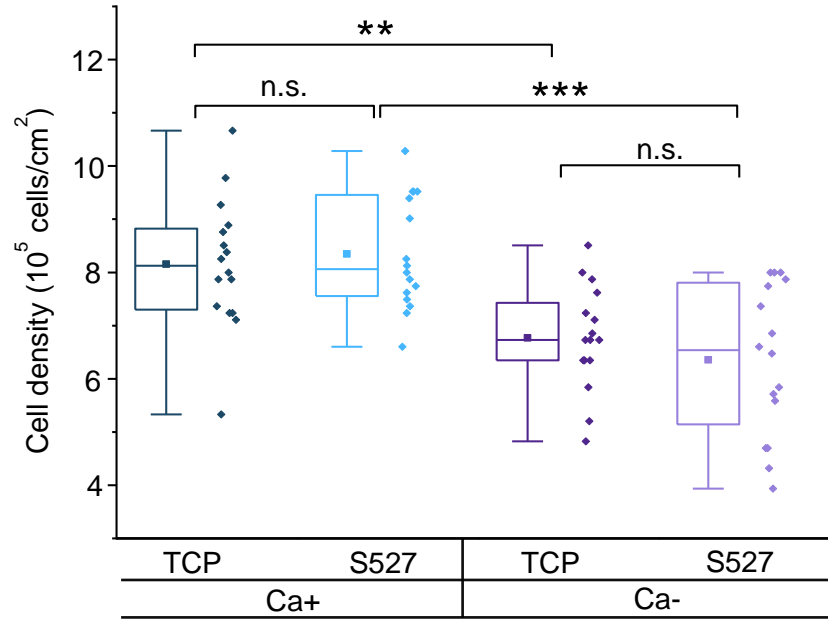
Figure S7: Density measurements were calculated by dividing phase contrast images of cells (previously used to quantify Fig. 2E-H) into 4X4 subfields and counting the total number of cells in each section. Substrate stiffness was not found to have a significant effect on cell density, which was instead governed by the calcium condition. Here, cells subject to calcium deficiency show decreased density.; n=16. * p≤0.05, ** p≤0.01, *** p≤0.001.
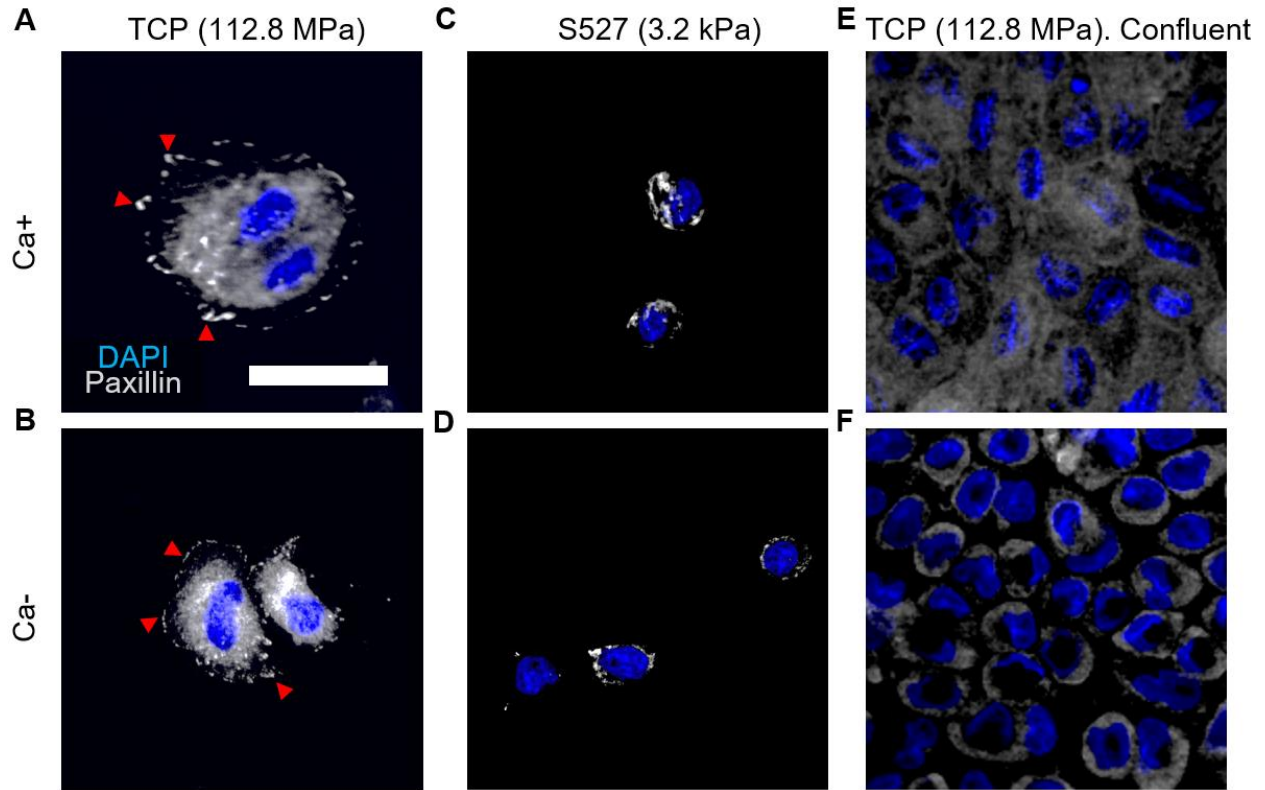
Figure S8: Immunofluorescence images of paxillin stained cells post Ca+/- treatment reveal that focal adhesion (FA) formation for (A,B) single cells grown on TCP, (C,D) single cells grown on S527, and (E,F) confluent cells grown on TCP is not significantly affected by calcium condition. For non-confluent samples, FA formation was instead governed by the substrate stiffness. Consistent with previous studies, TCP induced increased FA clusters around the cell periphery (5-7) and cell-spreading (8-10) compared to S527, regardless of calcium condition. However, FAs are shown to delocalize in a confluent cell layer. The process of cell-cell adhesions masking cell-substrate influence can be described using two-steps: 1) simultaneously, focal adhesions delocalize and cell-cell adhesions are established (Fig. S4) in confluent epithelium 2) cell-substrate interactions are reduced due to FA delocalization and cell morphology influence is then dominated by cell-cell interactions. This hypothesis is supported by previous works and numerical simulations. For example, cell mechanics experiments demonstrated that a free-standing MDCK monolayer can maintain cuboidal morphology in the absence of a substrate (8). The widely utilized vertex model also primarily relies on cell-cell contacts to determine cell shape and energy function (9-11). Scale bar = 30 microns.
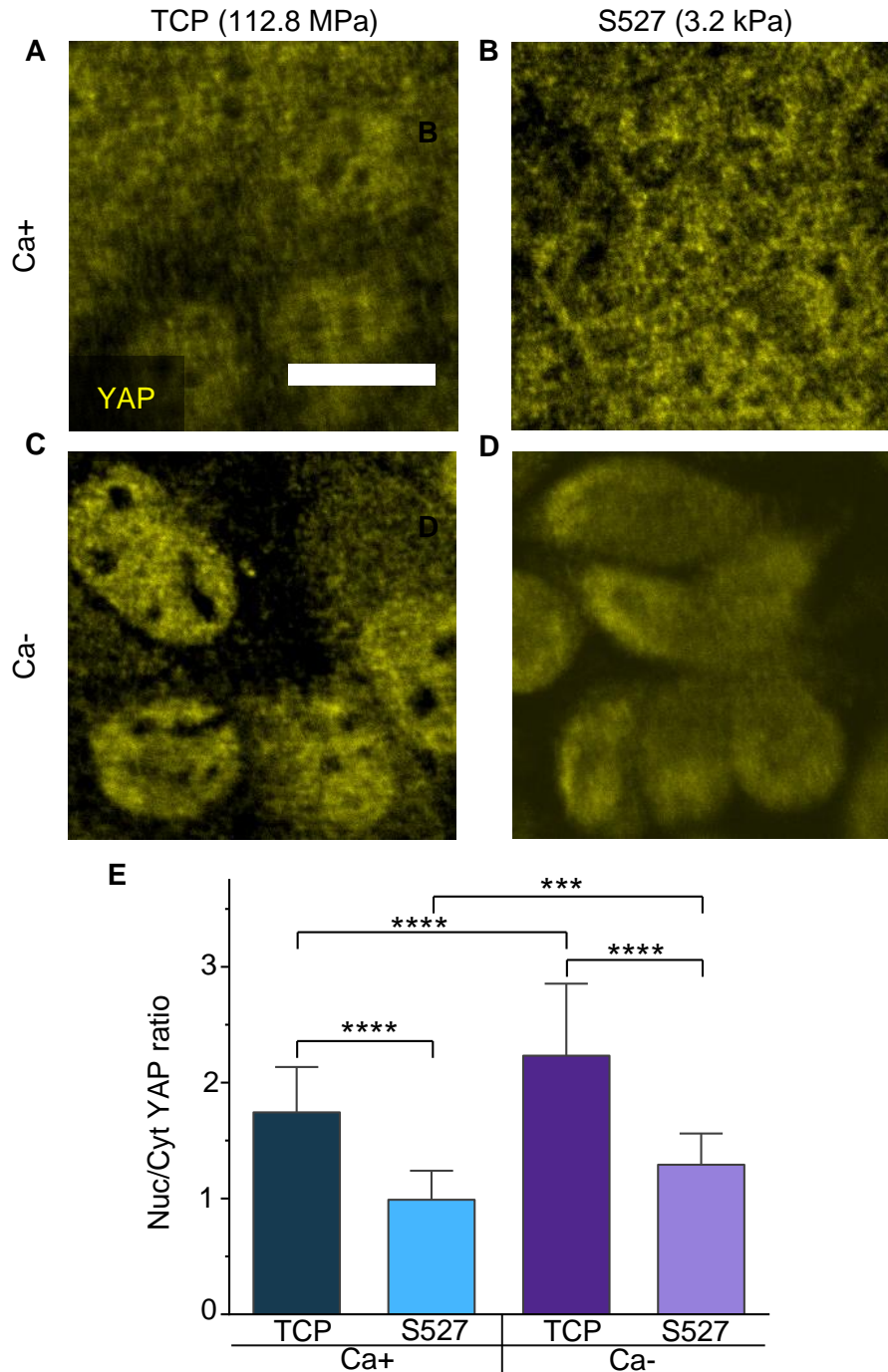
Figure S9: (A-D) Immunofluorescence images of YAP-stained cells were taken after the Ca+/- experiment. (E) Quantification of the nucleus/cytoplasm ratio reveals that cells grown on TCP have higher YAP activity compared to cells grown on S527. Additionally, calcium deficiency was shown to increase YAP activity. These results show a similar pattern to our reported SERPINE1 expression (Fig. 4), supporting our downstream gene expression results.; Scale bar = 15 microns. For (E), n=20. * p≤0.05, ** p≤0.01, *** p≤0.001, **** p≤0.0001.
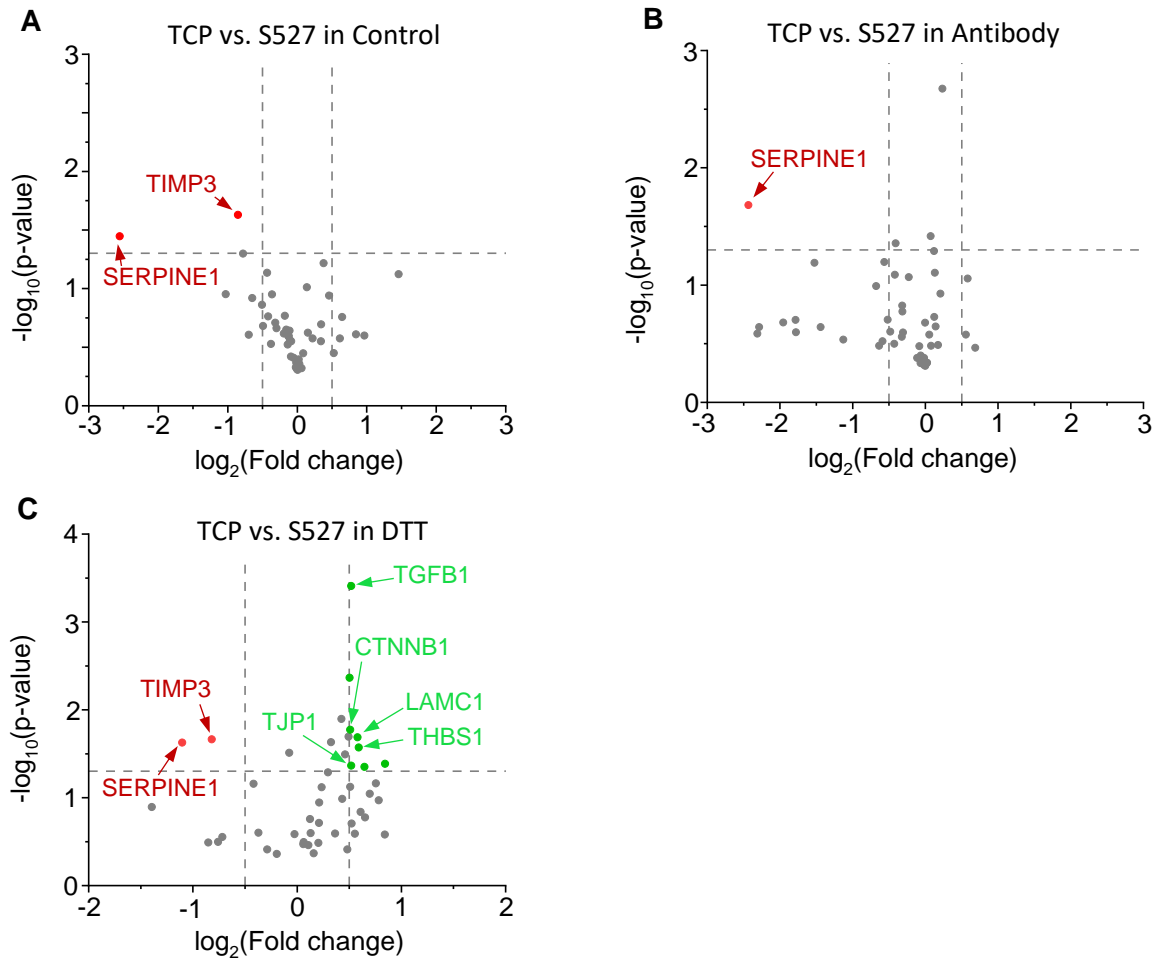
Figure S10: mRNA gene analysis was performed on all cultures for the antibody and DTT experiments and organized into volcano plots. The confluent control (A) was repeated to ensure consistent quality for all experiments. mRNA comparisons from antibody (B) and DTT (C) treatments show similar expressions to the Ca- experiment. Upregulation of other genes in the DTT condition may be due to other factors, such as the non-specific nature of DTT's disulfide exchange mechanism.
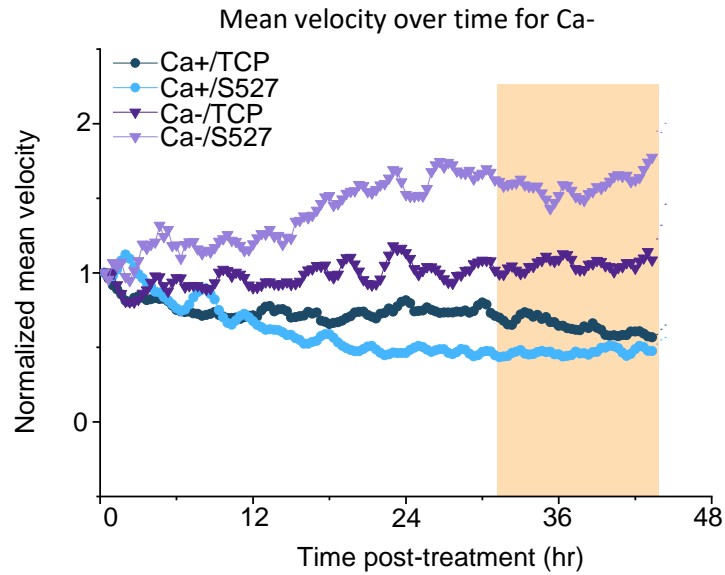
Figure S11: Mean cell velocity of predefined field of views were calculated using PIV. These values were normalized to visualize the differences in velocity by condition over time. Those treated with control media slowed over time, indicative of increased cell packing over time. Those treated with Ca- media increased in velocity over time, suggesting a loss of cell-cell communication. The coloured area represents the data points used for Fig. 6A.

EMT	Cell Adhesion	Epithelial Phenotype	Ion Transport	Solute Transport	Housekeeping
FN1	CDH1	FOS	ABCA5	SLC15A2	ACTB
COL1A1	CDH2	LIF	ABCB2	SLC1A1	GAPDH
LAMA5	CDH6	LRP2	ABCB3	SLC22A2	TBP
LAMB1	CLDN4	LTBP2	ABCB4	SLC25A5	
LAMC1	CTNNB1	PTGS2	ABCC2	SLC2A1	
SMAD3	ITGA2		ABCC4	SLC4A11	
SMAD7	ITGB4		ABCC5	SLC5A6	
TGFB1	TJP1		ABCD4	SLC6A12	
TGFBR1	MMP12		ABCG2		
TGIF1	MMP2				
THBS1	SERPINE1				
VIM	TIMP3				
SKIL					

Table S1: All genes that were tested via NanoString is listed and organized by type.

Down	Up
SERPINE1	FN1
	LAMB1
	LAMC1
	SMAD7
	TGFBR1
	THBS1
	SKIL
	CDH6
	ITGA2
	TJP1
	FOS
	PTGS2
	ABCA5
	ABCC4
	ABCC5
	SLC1A1
	SLC6A12

Table S2: This is a table of genes that were significantly down or up-regulated in Fig. 1D. Although only EMT genes were highlighted in the aforementioned figure, genes of all types were found to be upregulated.

References:

1. Sanches, João Miguel, et al., *European Journal of Human Genetics* 23.8 (2015): 1072-1079.
2. Hwang, Soonyean, et al., *Journal of Biological Chemistry* 287.26 (2012): 22227-22240.
3. Tokuo, Hiroshi, and Lynne M. Coluccio., *Molecular biology of the cell* 24.18 (2013): 2820-2833.
4. Ohama, Takashi, et al., *BMC cell biology* 14.1 (2013): 1-12.
5. Yeung, T., P. C. Georges, L. A. Flanagan, B. Marg, M. Ortiz, M. Funaki, N. Zahir, W. Ming, V. Weaver, and P. A. Janmey, 2005. Effects of substrate stiffness on cell morphology, cytoskeletal structure, and adhesion. Cell motility and the cytoskeleton 60:24–34.
6. Tee, S.-Y., J. Fu, C. S. Chen, and P. A. Janmey, 2011. Cell shape and substrate rigidity both regulate cell stiffness. Biophysical journal 100:L25–L27.
7. Saez, A., M. Ghibaudo, A. Buguin, P. Silberzan, and B. Ladoux, 2007. Rigidity-driven growth and migration of epithelial cells on microstructured anisotropic substrates. Proceedings of the National Academy of Sciences 104:8281–8286.
8. Harris, Andrew R., et al. "Characterizing the mechanics of cultured cell monolayers." *Proceedings of the National Academy of Sciences* 109.41 (2012): 16449-16454.
9. Nagai, T. & Honda, H. A dynamic cell model for the formation of epithelial tissues. *Phil. Mag. B* 81, 699–719 (2001).
10. Fletcher, Alexander G., et al. "Vertex models of epithelial morphogenesis." *Biophysical journal* 106.11 (2014): 2291-2304.
11. Bi, Dapeng, et al. "Motility-driven glass and jamming transitions in biological tissues." *Physical Review X* 6.2 (2016): 021011.